Biophysical Journal, Volume *112*

Supplemental Information

GsMTx4: Mechanism of Inhibiting Mechanosensitive Ion Channels

Radhakrishnan Gnanasambandam, Chiranjib Ghatak, Anthony Yasmann, Kazuhisa Nishizawa, Frederick Sachs, Alexey S. Ladokhin, Sergei I. Sukharev, and Thomas M. Suchyna

Methods

Fluorescence measurements of membrane binding: The interaction between these tryptophan-containing peptides and lipid vesicles was studied as described in (1). Briefly, tryptophan (Trp) fluorescence from 2 µM peptide was measured using a SPEX Flurolog FL 3-22 steady state fluorescence spectrometer (Jobin Yvon, Edison, NJ) equipped with double grating excitation and emission monochromators. Trp residues were excited at 280 nm and emission spectra were recorded between 290 nm and 500 nm using excitation and emission spectral slits of 2 and 4 nm, respectively. Measurements were made at 25°C in 2x10 mm cuvettes oriented perpendicular to the excitation beam. Quenching of Trp emission by aqueous iodide was measured in the presence of increasing concentrations of large unilamellar vesicles (LUVs) composed of either 1-palmitoyl-2-oleoyl-sn-glycero-3-phosphocholine (POPC) (Avanti, Alabaster, AL) or 25%POPC and 75% 1-palmitoyl-2-oleoyl-sn-glycero-3-phosphoglycerol (POPG). All spectra were recorded after equilibration of the sample. Corrections for background and the fitting of spectra were performed as previously described (2). Breifly, fluorescence intensities I, corrected for scattering
and dilution, were fitted to the following equation:

$$I([\mathrm{L}]) = 1 + I_{\max}\frac{K_x[\mathrm{L}]}{[\mathrm{W}] + K_x[\mathrm{L}]},$$

where I_{max} is the fluorescence increase on complete binding, [L] is the molar concentration of lipid, [W] is the molar concentration of water (55.3 M), and K_x is the mole fraction partition coefficient. The free energies of transfer from water to membrane were calculated from the mole fraction partition coefficients using

$$\Delta G = -RT\ln K_x.$$

Peptide depth estimates using aqueous and membrane resident quenchers: We used two types of quenching agents - water-soluble acrylamide and POPC:POPG vesicles made with the membrane resident 10-docylnonadecane (10-DN) quencher. Excitation and emission recording parameters were the same as above. Fluorescence was measured as increasing concentrations of the two quenching agents were added to 2 µM WT and different analog peptides.

1. Posokhov, Y. O., P. A. Gottlieb, and A. S. Ladokhin. 2007. Quenching-enhanced fluorescence titration protocol for accurate determination of free energy of membrane binding. Anal Biochem 362:290-292.
2. Ladokhin, A. S., S. Jayasinghe, and S. H. White. 2000. How to measure and analyze tryptophan fluorescence in membranes properly, and why bother? Anal Biochem 285:235-245.

CD spectrum of WT and K28E variant of GsMTx4 Peptides in Solution and Bound to Membranes

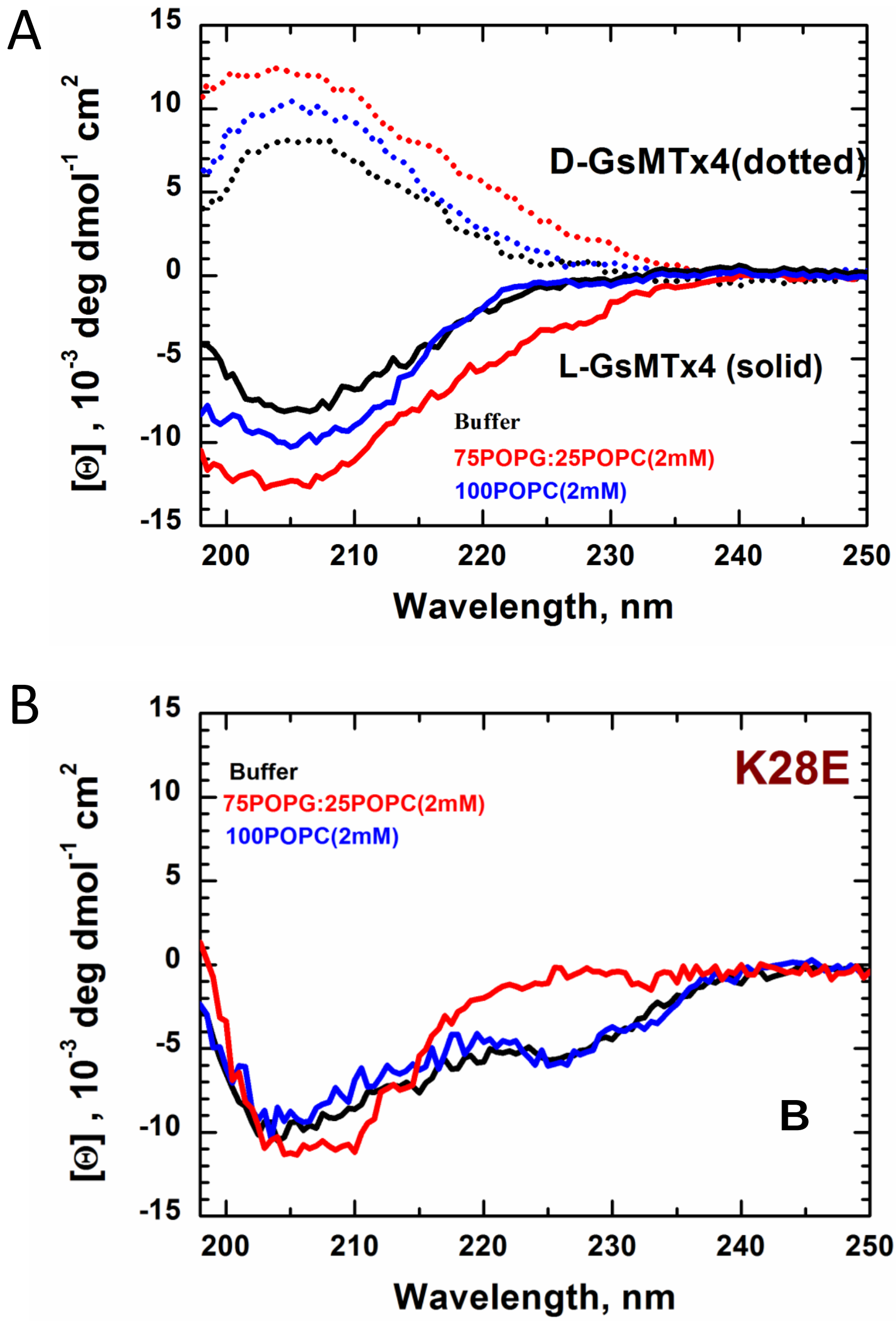

Figure S1. Representative CD spectrum of the D and L enantiomers of WT GsMTx4 (A) and the GsMTx4 K28E variant (B) in 10 mM $NaPO_4$ buffer pH 7.4, 3:1 POPG:POPC (anionic) and POPC (zwitterionic) vesicles. The negative peak at 228 nm present in the K28E variant disappears when bound to anionic, but not zwitterionic, vesicles. (n=2/peptide)

Supporting Figure S1

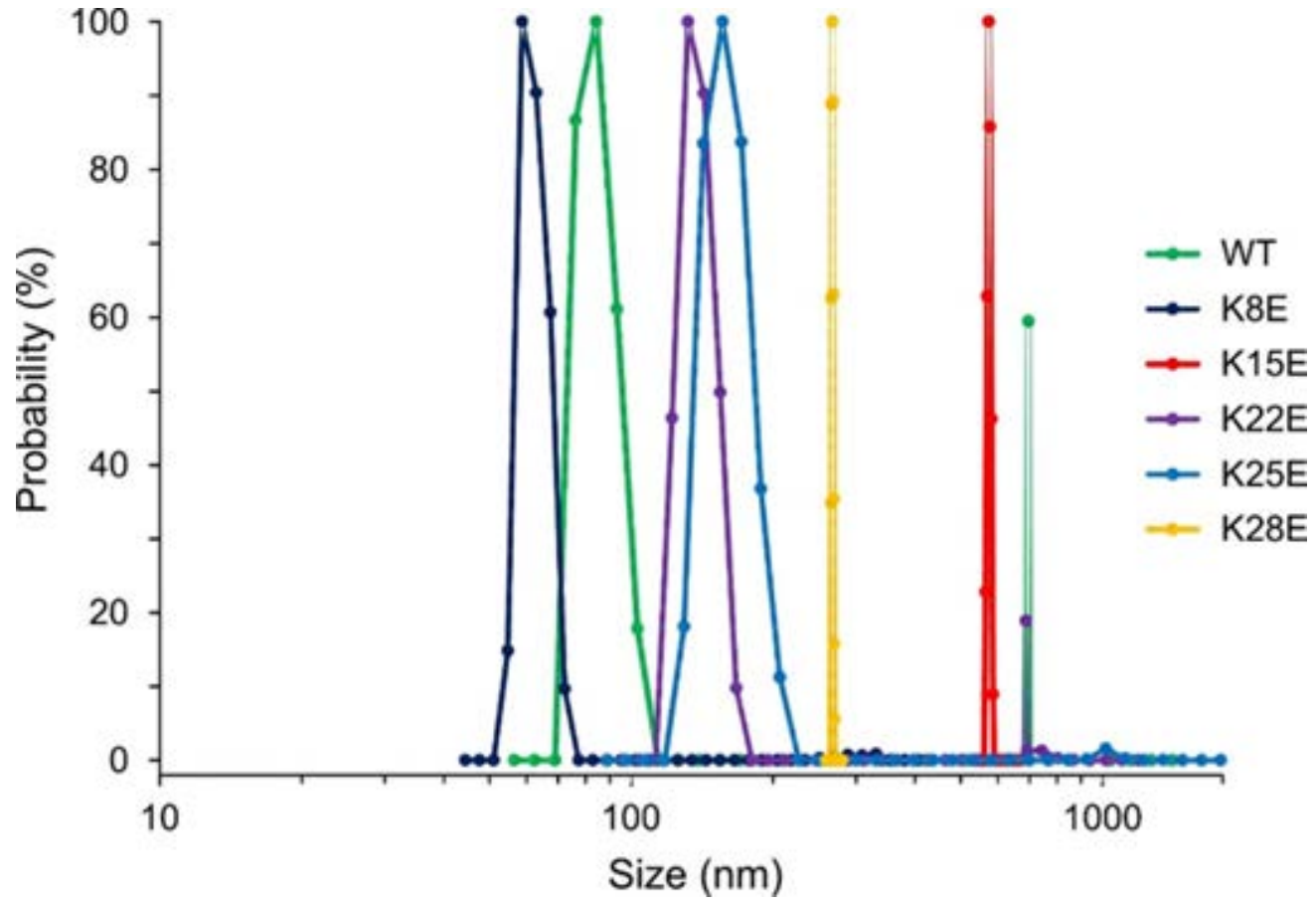

Figure S2. The distributions of particle size measured by Dynamic Light Scattering in solutions of WT GsMTx4 and four variants at 30 μM. The distributions show the K-E mutations produce different aggregation sizes for the peptides in aqueous solution. The least active peptide K15E shows the largest aggregates, while WT and the uncompromised K8E show the smallest aggregation sizes.

Dynamic light scattering analysis of peptide aggregation: Peptide aggregation is suggested by the CD results and aggregation can reduce the effective concentration (activity) of the peptide. It can also modify the partitioning of the peptide with the membrane. The aggregation properties were investigated using DLS. DLS experiments were performed with 30 μM WT or variant peptides, and the volume placed in the cuvette was 1.0 mL. All variants were tested independently three times. All peptides showed aggregate particle sizes represented by single peaks of 50-400 nm in size (Fig. 12), corresponding to aggregation numbers between 1.6×10^4 for K8E and 1.4×10^7 for the most compromised K15E variant (assuming that molecular volume of GsMTx4 is ~6.7 nm^3/monomer). Only WT and K22E peptides showed smaller peaks of larger particles near 700 nm, whereas the main peak for K15E particles was near 570 nm. It is obvious that inactive variants form larger aggregates at 30 μM which may lower the effective peptide concentration. We should note that the monomer-aggregate equilibrium is concentration-dependent (see Figure S3), but the sensitivity to aggregate sizes was too low at 3 μM. To increase the intensity of scattered light we used about an order of magnitude higher concentration than in the electrophysiological experiments.

Methods: These experiments examined the tendency of the peptides to aggregate. The peptides were diluted to 20 mM in the standard 50 mM KCl buffer and within one hour were subjected to dynamic light scattering (DLS) measurements on a 90 Plus Particle Size Analyzer (Brookhaven Instruments Corp.) pre-calibrated with 92nm nanospheres (Duke Scientific Corp.). Autocorrelation data were collected during five 1-min intervals and averaged.

Supporting Figure S2

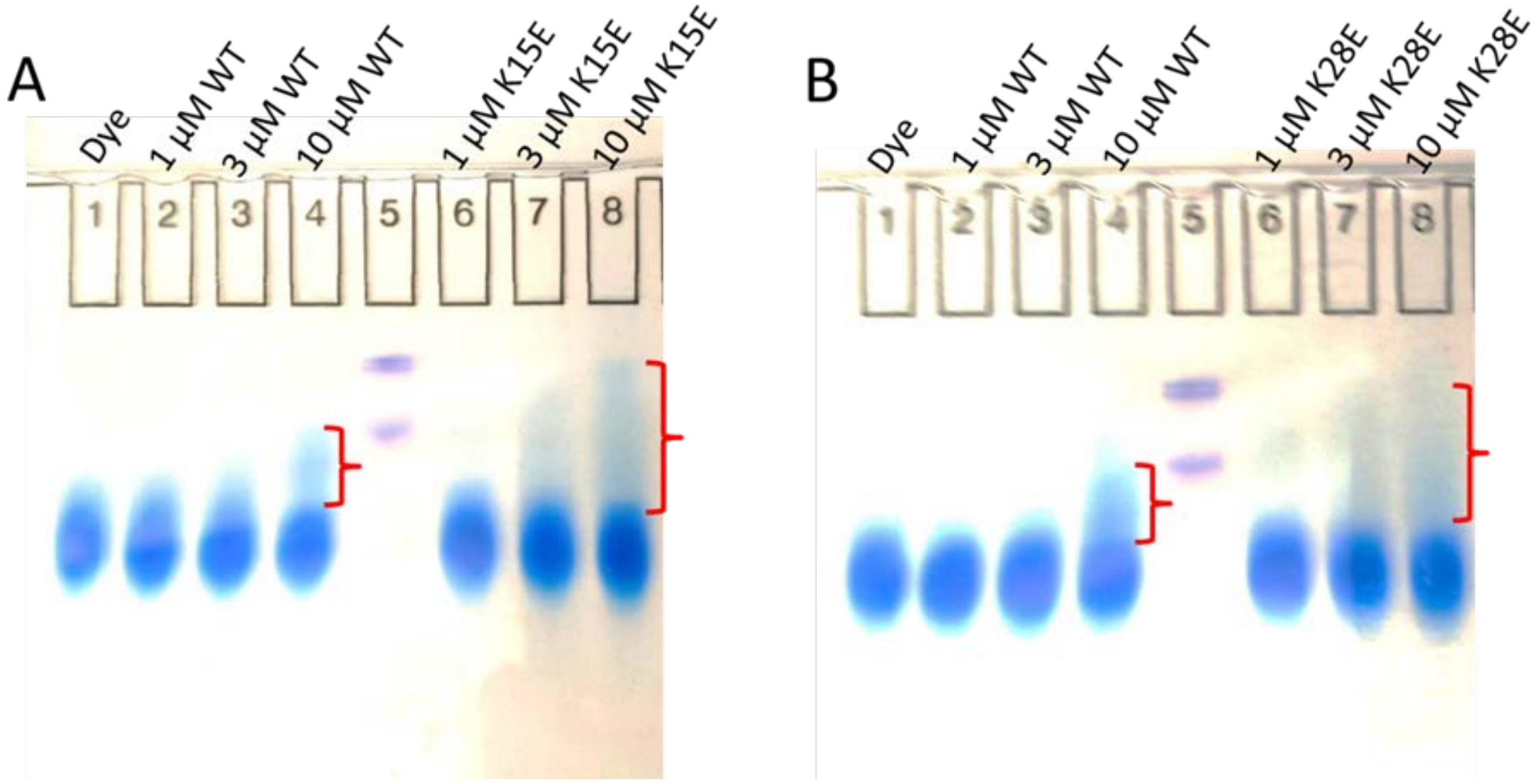

Figure S3. GsMTx4 WT and either K15E (A) or K28E (B) variants run by nondenaturing PAGE suggesting peptide aggregation at higher concentrations. Three concentrations for each peptide show that aggregate size increases with concentration, and that the aggregate sizes are larger for the variants than WT (red brackets). However, at 1 µM there is little evidence of aggregation. This is not due to sensitivity since we are able to detect <10 ng of protein with G250 dye (1 µM = 40 ng of protein in 10 µl).

Non-denaturing gel electrophoresis analysis of peptide aggregation: To determine the concentration dependence of aggregation size at lower concentrations, we ran WT, K15E, and K28E at 1, 3, and 10 µM on non-denaturing gels to estimate particle sizes. SDS denatured samples of 10 µM WT and variant peptides dissociated into the 4096 Da monomeric form and all material ran with G250 dye in the loading buffer. However, under non-denaturing conditions we observed results similar to those observed in the DLS experiments, where larger aggregates (slowly migrating) were present for the variants compared to the WT peptide (Fig. S3). Aggregate sizes were concentration dependent with no visible aggregates detected at 1 µM (40 ng of peptide), and only weakly retarded species at 3 µM. Significantly larger aggregates were observed at 10 µM. Due to the non-denaturing conditions we were unable to determine the aggregate sizes, but clearly some aggregation is occurring at lower concentrations and users should be mindful of this property.

Methods: : Three concentrations (1, 3 and 10 µM) of WT peptide and variant peptides (K8E and K28E) were run on 10-20% gradients of Tris/Tricine polyacrylamide gels from Biorad. The gels were run at 100 V and 400 mA for 1 hour. The markers were Precision Plus dual extra protein standard marker from Biorad containing SDS. Tris Tricine running buffer contained 100 mM Tris and 100 mM Tricine at pH 8.3. Tricine loading buffer contained 100 mM TrisCl, pH 8.3, 30% glycerol, and 0.25% Coomassie Brilliant blue G 250. The G250 stain is sensitive to 10 ng of protein.

Supporting Figure S3

A

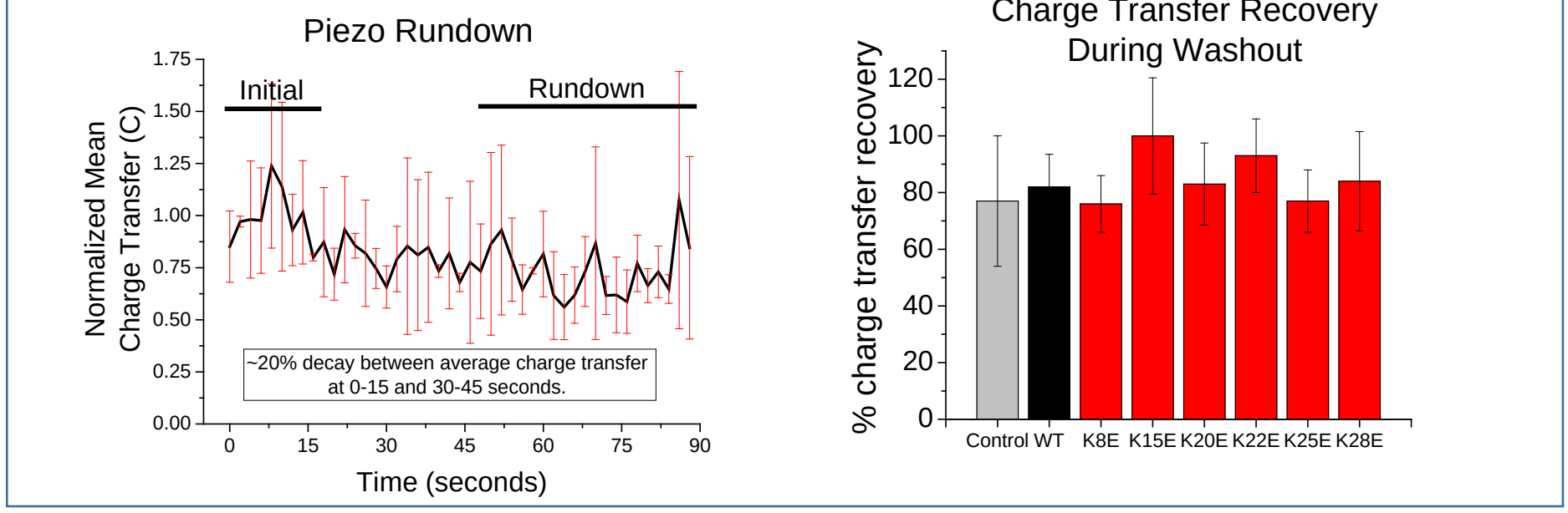

B

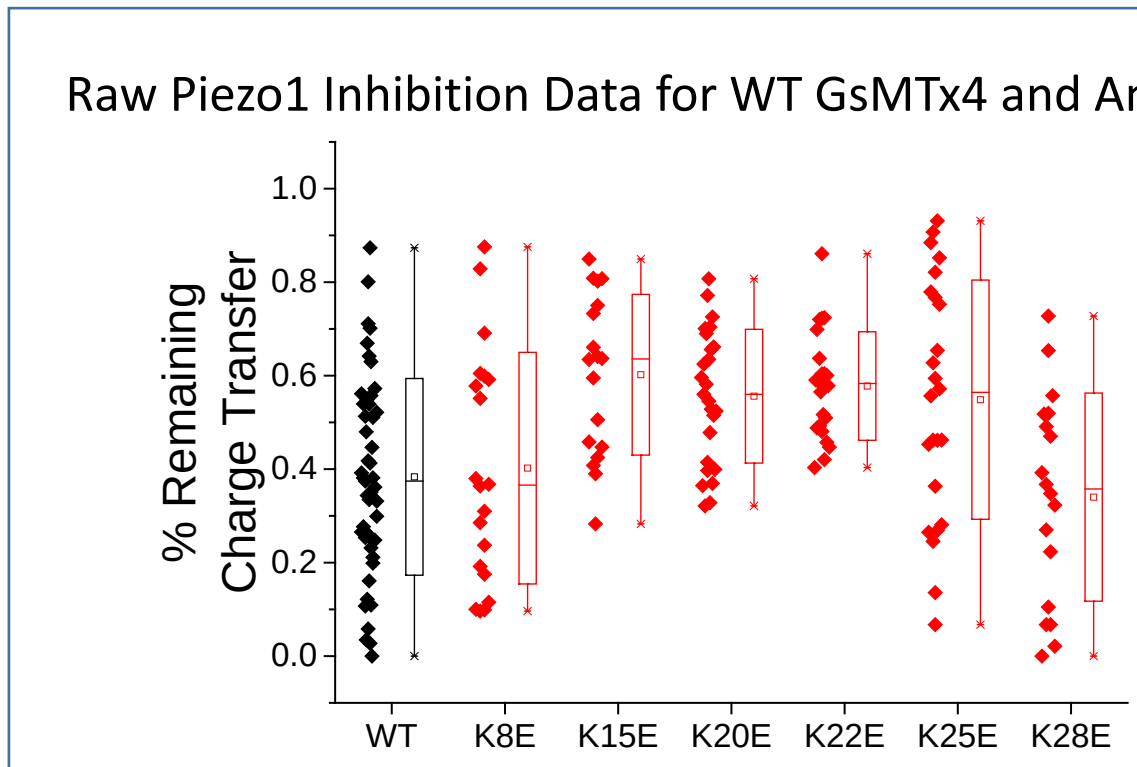

Figure S4. Summary of channel rundown, recovery and inhibition strength from peptide application. (**A**) The trace in the left panel shows the mean charge transfer from n=3 patches in normal saline expressing piezo channels monitored over 1.5 min to determine the rate of rundown. Pressure steps were applied every 2 seconds. The mean charge transfer over the first 20s (*Initial* black line) was set as 100% and the amount of rundown was assessed by normalizing the charge transfer that occurred between 60-90s (*Rundown* black line) to this initial level. The bar graph in the right panel shows there was ~20% rundown over 75 seconds which is shown by the control (gray) bar. Most tests of peptide inhibition on Piezo channels took ~75 seconds for the decay and recovery phases to be measured. The recovery levels after washout of the different peptide analogs was consistent with this level of rundown in the control patches. (**B**). The time for application and washout generally took 60-90 seconds and the levels of charge transfer recovery following washout of the different analogs were similar to the control level. This suggests that nearly complete washout of the peptides occurred after 20 seconds of wash time. (**C**) Summary of percent charge transfer reduction for all patches used in the inhibition potency tests of WT (black) and analog (red) peptides. Box plots for each peptide tested were generated from the fractional remaining steady state decay current for each patch shown to the left of the boxes (number of patches for each peptide were WT=47, K8E=20, K15E=18, K20E=25, K22E=22, K25E=24, K28E=18). The ends of the boxes represent 1 SD from the mean designated by (▫). The line through the box is the median and the extended lines ended with x at the ends designate the range of the data.

Supporting Figure S4

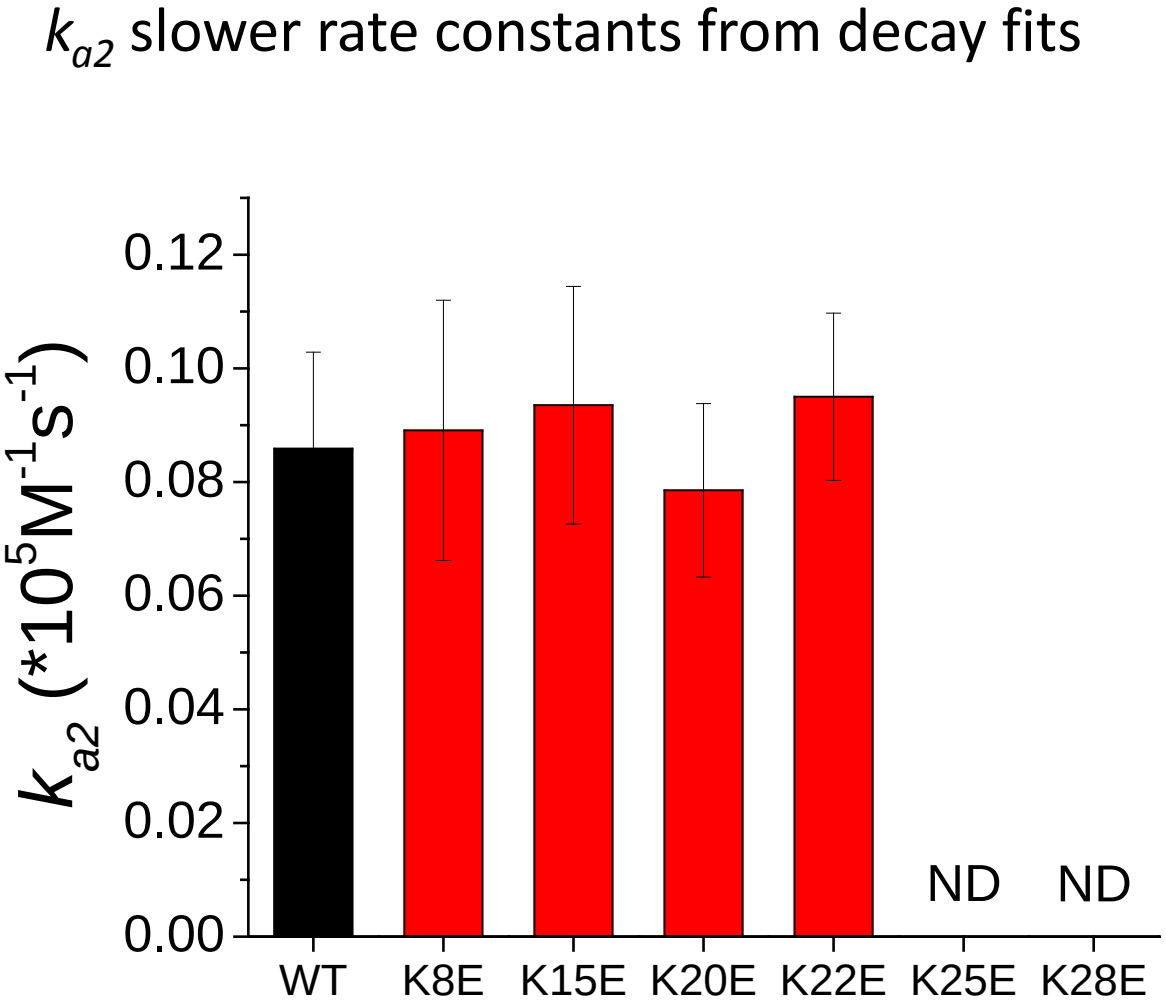

Figure S5. For all peptides, >50% of patch data showed current decays that were modeled best using two time constants as shown in Fig. 2C. The k_a values calculated from the second (slower) decay time constant shows no difference between the variants and WT peptide. The number of patches for each peptide were WT=15, K8E=12, K15E=12, K20E=16, K22E=12). K25E and K28E were not determined (ND) because too few patch data sets produced acceptable fits for the second time constant.

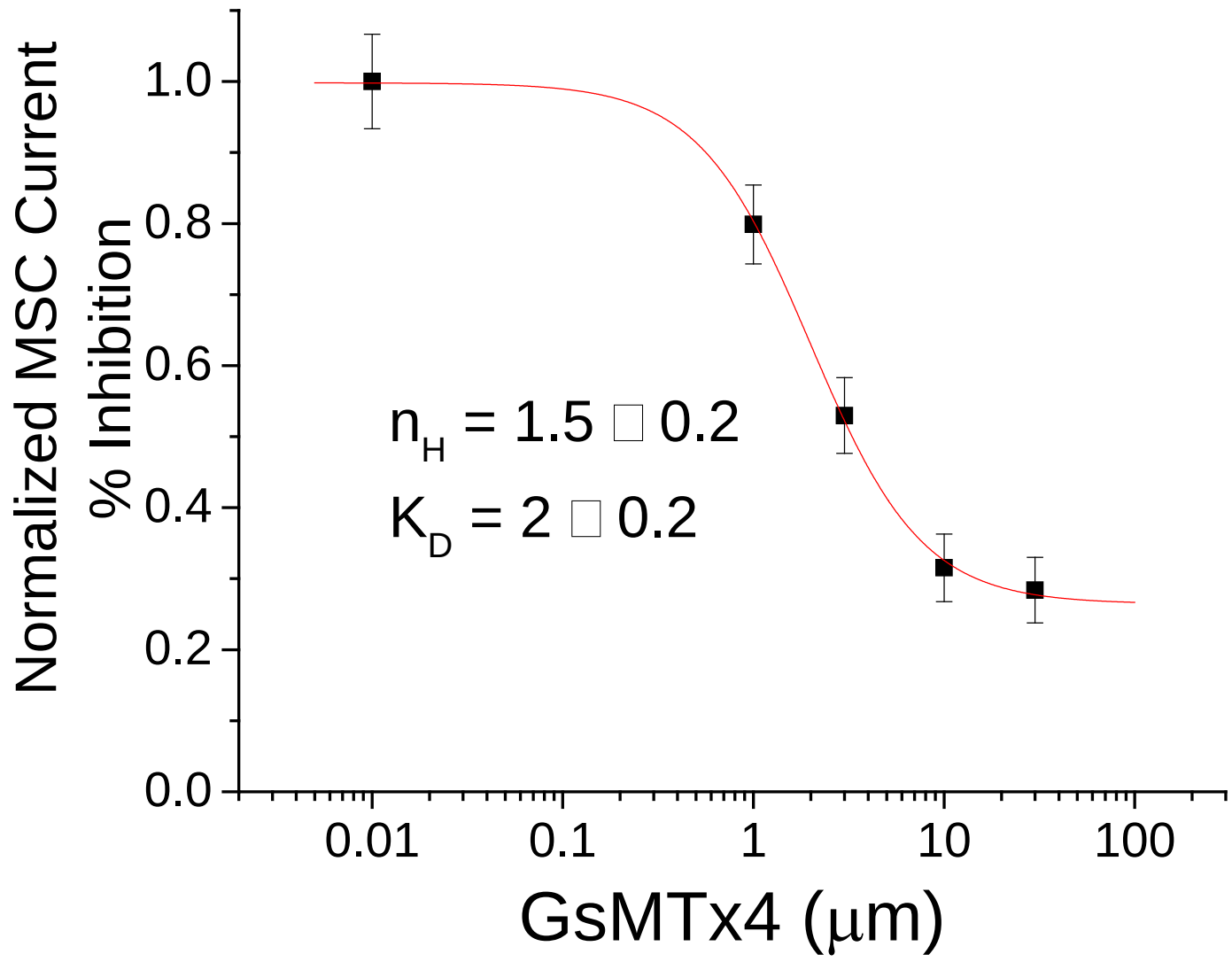

Figure S6. Concentration dependence of inhibition by WT GsMTx4. Each point represents the average Piezo1 current from 7-12 patches in the presence of the indicated GsMTx4 concentration. Red curve shows the Hill equation fit to the data. The K_D's determined here are slightly higher than the previously determined K_D (~0.5 μM) (1,2) likely due to differences in the pressure step protocols used in the different studies. The Hill coefficient was 1.5, suggesting that inhibition may involve more than one peptide. Interestingly, MD simulations predict that stable dimer formation occurs at resting tension between a membrane bound and a second unbound GsMTx4 peptide, and that the second peptide dissolves rapidly into the membrane upon an increase in tension (3).

1. **Suchyna, T. M., J. H. Johnson, H. F. Clemo, Z. H. Huang, D. A. Gage, C. M. Baumgarten, and F. Sachs. 2000. Identification of a peptide toxin from Grammostola spatulata spider venom that blocks stretch activated channels. Journal of General Physiology 115:583-598.**
2. **Bae, C., F. Sachs, and P. A. Gottlieb. 2011. The mechanosensitive ion channel Piezo1 is inhibited by the peptide GsMTx4. Biochemistry 50:6295-6300.**
3. **Nishizawa, K., M. Nishizawa, R. Gnanasambandam, F. Sachs, S. I. Sukharev, and T. M. Suchyna. 2015. Effects of Lys to Glu mutations in GsMTx4 on membrane binding, peptide orientation, and self-association propensity, as analyzed by molecular dynamics simulations. Biochimica et Biophysica Acta (BBA)-Biomembranes.**

TREK1 Currents Potentiated by GSMTx4

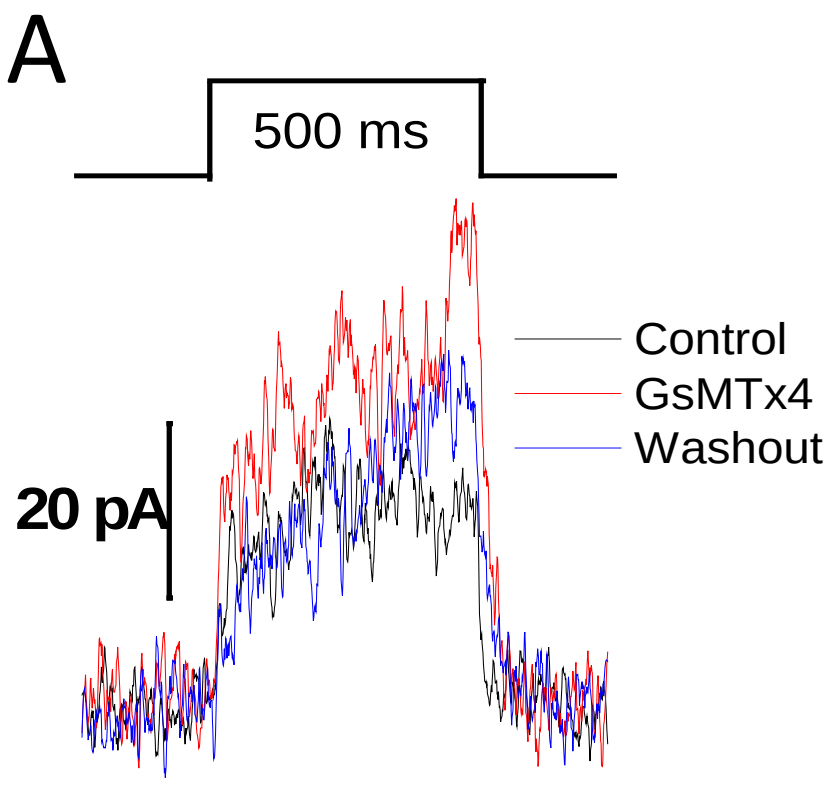

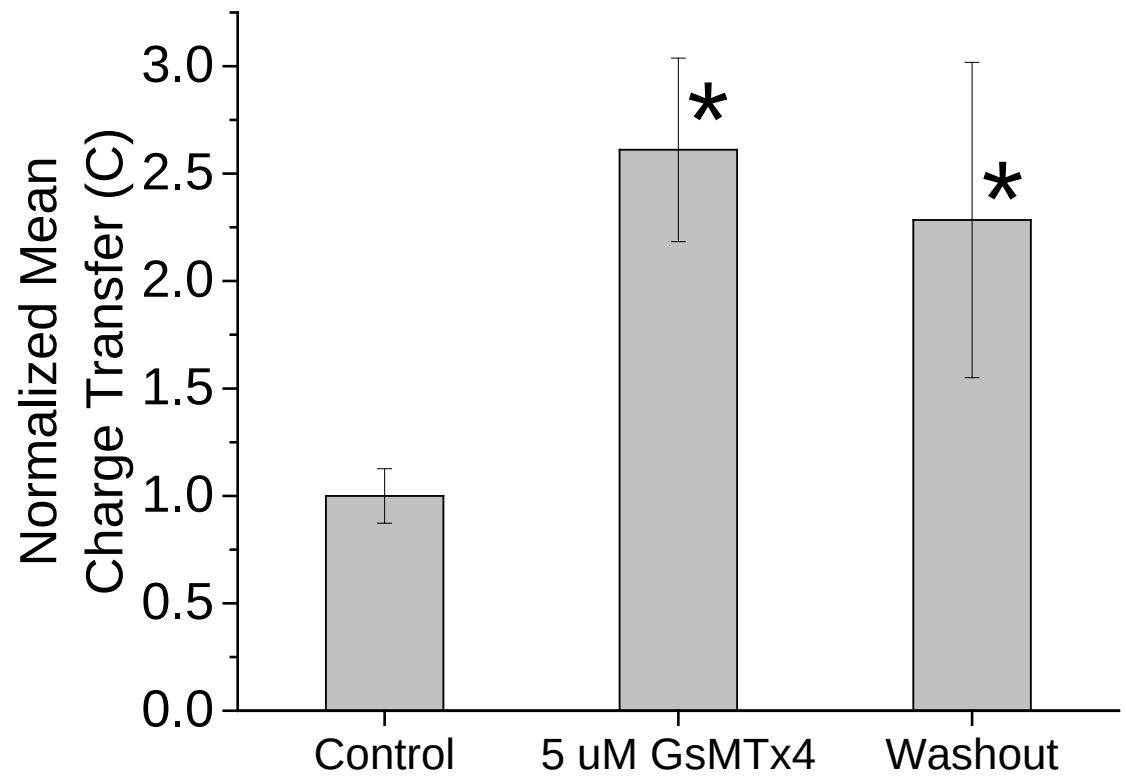

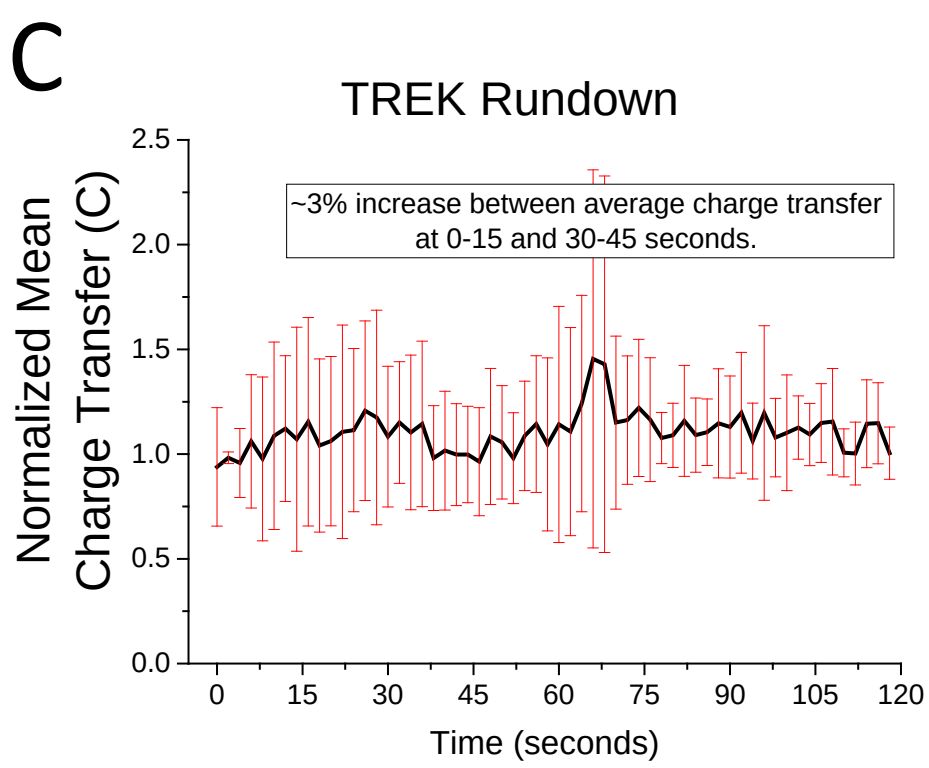

Figure S7. TREK1 channel currents are potentiated by GsMTx4. TREK 1 currents from HEK cell outside-out patches were observed in increase when 5 µM GsMTx4 was applied **(A)**. Representative traces show TREK1 currents did not inactivate during a pressure step and were also active during the intervening unstretched time between pressure steps as shown by the greater noise level of the baseline compared to Piezo1 currents in Figure 2. GsMTx4 produced an average 2.6±0.06 fold increase in activity (n=6 patches) that did not decrease significantly after 60 seconds of washout **(B)** (* denotes significantly different from control current at $\alpha = 0.05$). **(C)** Mean charge transfer from three TREK 1 expressing patches showed no rundown over two minutes of constant stimulation in normal bath saline.

Methods: HEK293 cells were transfected with 0.5-1 µg of TREK cDNA expression vector containing a GFP indicator of transfection. For recordings of TREK channels, the bath solution contained (in mM): 150 KCl, 1 $CaCl_2$, 1 $MgCl_2$, 10 HEPES and the pipette solution contained 150 KCl, 10 HEPES. The pH of these TREK channel recording solutions were adjusted to 7.4. We used protocols identical to those used for activation of Piezo channels to activate TREK channels; they were activated at 50 mV and 40-90 mmHg.

Supporting Figure S7

Peptide-vesicle affinity determined by isothermal titration calorimetry:

Peptide	N1	K1 (M^{-1})	ΔH1 (Cal/mol)	ΔS1 (Cal/mol·K)	N2	K2 (M^{-1})	ΔH2 (Cal/mol)	ΔS2 (Cal/mol·K)
L-GsMTx4	1.9±0.6	(2.4±1.2)E5	-1078±470	21.2±2.0	2.4±0.9	(2.7±1.6)E6	-1565±96	24.2±0.8
K8E	0.4±0.1	(8.0±3.2)E4	-1580±80	17.2±2.2	0.8±0.2	(8.8±1.6)E6	-1530±120	26.6±1.2
K15E	0.2±0.1	(8.6±4.3)E6	5150±2020	63±20	0.8±01	(2.2±1.2)E7	-5073±480	16.5±1.0
K22E	1.9±0.8	(2.3±1.6)E5	-934±202	21.5±1.4	3.1±1.1	(5.4±3.6)E6	-1500±20	25.8±0.2
K25E	1.4±0.2	(2.4±1.1)E5	-448±257	20.1±3.2	2.4±1.2	(3.1±1.1)E7	-773±110	28.6±3.2
K28E	1.3±0.5	(8.3±3.2)E5	-690±180	23.2±1.8	0.9±0.3	(2.1±0.7)E7	-903±85	30±0.7

Table S1. ITC Fitting Parameters. Based on the density values (N1 and N2), the low- and high-affinity sites occur in comparable amounts/densities. Of the two most compromised variants, K25E shows the highest K_2, and the K15E has positive ΔH1 and high ΔS1 suggesting that the low-affinity binding mode is different for this variant. The high-affinity binding mode for K15E variant is also characterized by unusually large negative enthalpy ΔH2. Each titration was repeated at least 3 times. The parameters are shown as mean ± SD.

A

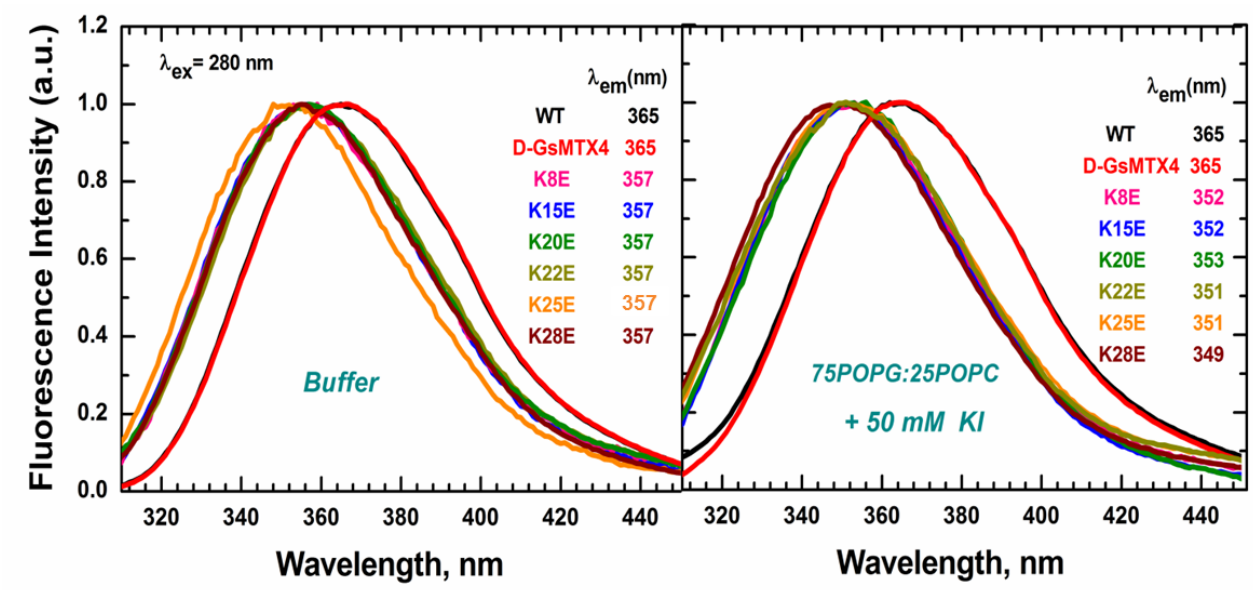

B

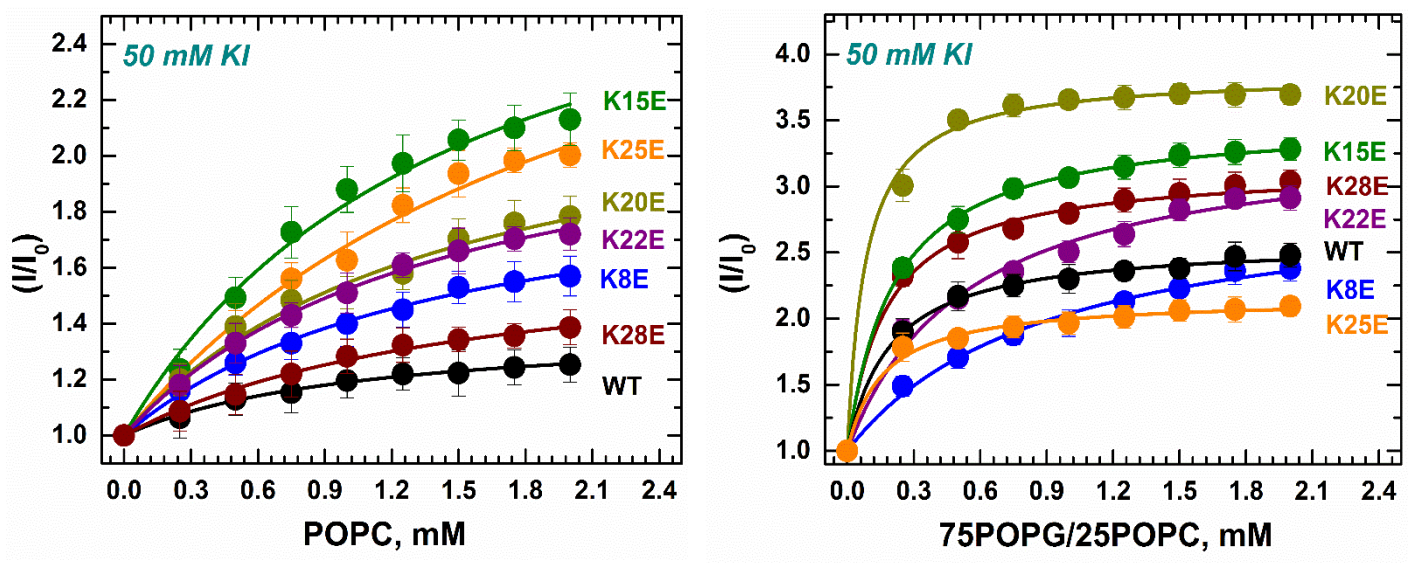

Figure S8. (A) Representative tryptophan fluorescence spectrums for GsMTx4 WT and K-E variants in solution (peptide concentration 2 µM) containing KI (first panel) and in the presences of 75POPG:25POPC LUVs (n=2 tests per variant). All variants had a pronounced ~8 nm blue shift compared to the D and L enantiomeric WT forms of GsMTx4 in solution. The blue shift for the variants was even more pronounced when bound to the POPG-POPC vesicles, but the WT peptides were unaffected. **(B)** Shows Trp fluorescence intensity curves for the different peptides titrated using increasing concentration of POPC or POPG-POPC LUV in the presence of aqueous 50 mM KI (n=3/variant). As the LUV concentration increases, peptide association with the membrane increases leading to protection of Trp quenching by aqueous iodine. Significantly higher concentrations of zwitterionic POPC LUV are required (first panel) to titrate the KI quenching compared to anionic POPG-POPC LUVs (second panel), and maximum protection levels for POPG:POPC were greater. Fitting of the titration data with a partitioning model suggests that the free energy of partitioning ΔG for all variants were similar to that of WT GsMTx4 for either LUV composition, but the values of the final intensity increase (Imax) were generally higher in variants suggesting lesser accessibility of Trps to quencher in membrane bound state.

Lipid titration of Trp quenching: GsMTx4 has two adjacent Trp residues that have a peak emission intensity at 365 nm in solution and were unaffected by binding to LUVs (Fig. S8A). The K-E variants all showed a peak emission intensity that was blue shifted ~8nm from WT in solution, suggesting a common effect of net charge on the Trp's environment. The blue shift is correlated with a more hydrophobic environment which, in solution, likely represents enhanced peptide aggregation that partially shields the Trp residues from the aqueous environment (see enhanced aggregation in Supporting Figs. S2 and S3). As shown previously (1), both the D and L enantiomers of WT GsMTx4 were not blue shifted in the presence of either POPC or POPG-POPC LUVs (Fig. S8A, second panel and Table S2). The variants all showed a blue shift in the presence of POPG-POPC LUV, but not POPC (Supporting Fig. S8A and Table S2). We suggested that the lack of blue shift for the WT and D-enantiomer may be related to incomplete dehydration of the Trp residues upon binding (1). The presence of the shift for the variants in anionic vesicles suggests a more hydrophobic environment for the Trps, possibly related to a deeper penetration than WT.

The significant differences in I_{max} for the different peptides may represent differences quenching between membrane bound and aggregate fractions, or differences in peptide tilt, penetration depth and local lipid packing. There was a general trend for most variants to have higher I_{max} values than WT.

1. Posokhov, Y. O., P. A. Gottlieb, and A. S. Ladokhin. 2007. Quenching-enhanced fluorescence titration protocol for accurate determination of free energy of membrane binding. Anal Biochem 362:290-292.
2. Suchyna, T. M., J. H. Johnson, H. F. Clemo, Z. H. Huang, D. A. Gage, C. M. Baumgarten, and F. Sachs. 2000. Identification of a peptide toxin from Grammostola spatulata spider venom that blocks stretch activated channels. Journal of General Physiology 115:583-598.

Peptides	Fluorescence λ_{max} (nm) （± 1 nm）			ΔG, kJ/mole		I_{max}		Z_{eff}
	Buffer	100% POPC	75% POPG 25% POPC	100% POPC	75% POPG 25% POPC	100% POPC	75% POPG 25% POPC	
L-GsMTx4	365	365	365	-26.9 ± 0.3	-31.1 ± 0.2	1.4 ± 0.1	2.6 ± 0.1	+0.5
K8E	357	357	352	-26.2 ± 0.3	-27.3 ± 0.3	2.0 ± 0.1	3.0 ± 0.1	+0.2
K15E	357	357	352	-26.1 ± 0.4	-30.9 ± 0.1	3.1 ± 0.2	3.5 ± 0.1	+0.5
K20E	357	357	353	-26.2 ± 0.5	-33.3 ± 0.4	2.3 ±0.2	3.8 ± 0.1	+0.8
K22E	357	357	351	-26.2 ± 0.5	-28.6 ± 0.3	2.3 ±0.1	3.4 ± 0.1	+0.3
K25E	357	357	351	-25.1 ± 0.5	-31.6 ± 0.4	3.2 ±0.2	2.2 ± 0.1	+0.7
K28E	357	357	349	-25.9 ± 0.4	-31.4 ± 0.3	1.7 ±0.1	3.2 ± 0.1	+0.6

Table S2. Trp fluorescence changes associated with K-E variants and vesicle binding (partitioning model fitting parameters = means ± SE, n=3/peptide).

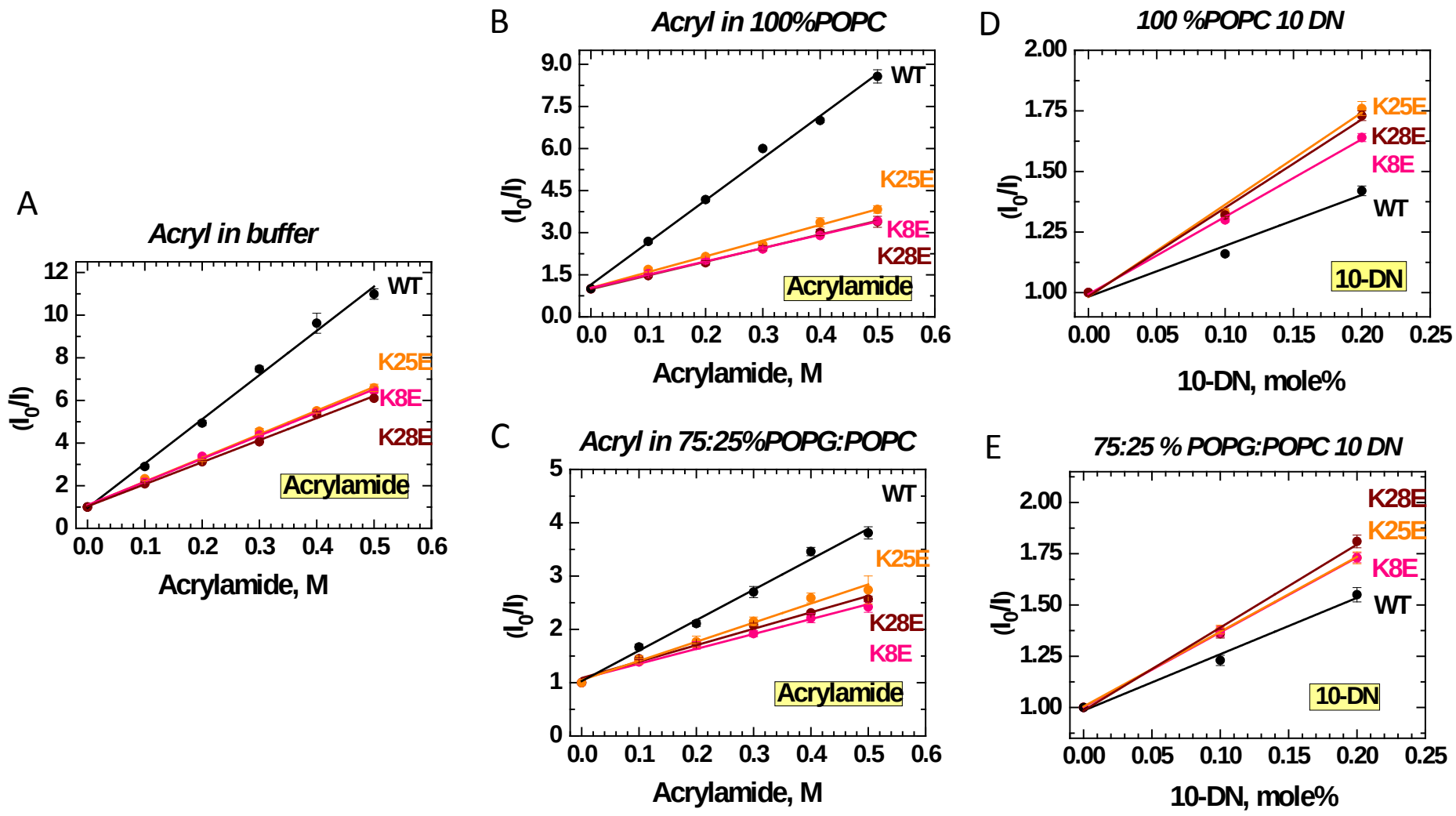

Figure S9. Acrylamide versus 10-DN quenching (K_{SV}) was used to compare penetration depth of WT and three different K-E variants at 2 µM peptide. (A) Shows the ratio of the initial fluorescent intensity to the quenched intensity (I_o/I, means±SE) for WT GsMTx4, and K8E, K25E, and K28E variants vs the concentration of Acrylamide (λ_{ex} = 295 nm). Spectra for these peptides in the presence of either 100% POPC (B) or 75%POPG:25%POPC (C) are corrected for the inner filter effect determined in buffer alone. The quenching is linearly related to the quenching agent concentration. The color coded KSV values in buffer and in the presence of the different types of LUVs is shown above the quenching data. The I_o/I for WT and variant peptides vs the concentration of the bilayer resident 10-DN quenching agent (λ_{ex} = 280 nm) is shown for POPC (D) and POPG/POPC (E) vesicles. At these concentrations quenching is linearly related to the concentration. All data sets are from n=3 tests.

Peptides	Buffer	Acrylamide 100%POPC	Acrylamide 75:25% POPG:POPC	10-DN 100%POPC	10-DN 75:25% POPG:POPC
WT	20.8 ± 0.7	15.0 ± 0.5	5.7 ± 0.2	2.1 ± 0.3	2.8 ± 0.3
K8E	10.8 ± 0.2	4.7 ± 0.1	2.8 ± 0.1	3.2 ± 0.1	3.7 ± 0.3
K25E	11.1 ± 0.3	5.6 ± 0.2	3.6 ± 0.2	3.8 ± 0.2	3.7 ± 0.1
K28E	10.3 ± 0.3	4.9 ± 0.1	3.1 ± 0.2	3.7 ± 0.3	4.1 ± 0.3

Table S3. Stern-Volmer quenching constant (KSV) calculated from the slopes of Trp fluorescence quenching data in Fig. S9. KSV values for water the soluble quencher acrylamide are expressed in units of M-1 and for membrane soluble 10-DN in dimensionless units. All values are means±SE (n=3) with * denoting statistically different Stern-Volmer constants from WT (α = 0.05).

Peptide depth analysis: Dual quenching analysis of peptides with two different quenching agents residing either in solution or in the membrane was compared to the brominated lipid method (Fig. S9). Acrylamide was the *aqueous* quencher that is unable to quench the fluorescence of residues deeply embedded in the bilayer (Fig. S9A, B and C). The other is 10-doxylnonadecane (10-DN) that is hydrophobic and efficiently quenches Trp residues residing near the bilayer center. The slope of the plot of quenching agent concentration vs the ratio of quenched fluorescence is the Stern-Volmer quenching constant (K_{SV}).

Trp fluorescence decreased linearly as the concentration of acrylamide increased in saline (Fig. 9A), or when peptides were bound to LUVs of POPC (Fig. 9B) or POPG-POPC (Fig. 9C). Quenching was greater in saline than in the presence of vesicles confirming membrane binding. ***However, the variants also showed significantly greater quenching in solution.*** The sensitivity of Trp fluorescence to 10-DN incorporated in POPC (Fig. 9D) and POPG-POPC (Fig. 9E) was also concentration dependent, but with a much shallower slope. Comparing the quenching constants of the three K-E variants to WT in the membrane-bound state (Table S3) shows that the variants have lower accessibility for water-soluble acrylamide and higher accessibility to membrane-soluble 10-DN suggesting increased shielding of variant Trp residues. However, Trp fluorescence in the variants is more strongly shielded in solution (likely due to greater aggregation), and this may contribute to the significantly greater shielding in the presence of lipids. Aggregation shielding contributions may exaggerate the difference between the variants and WT peptide and making it difficult to interpret the depth differences by this method.

Supporting Figure S9 and Table S3

Membrane Area Occupied by WT and Variant Peptides

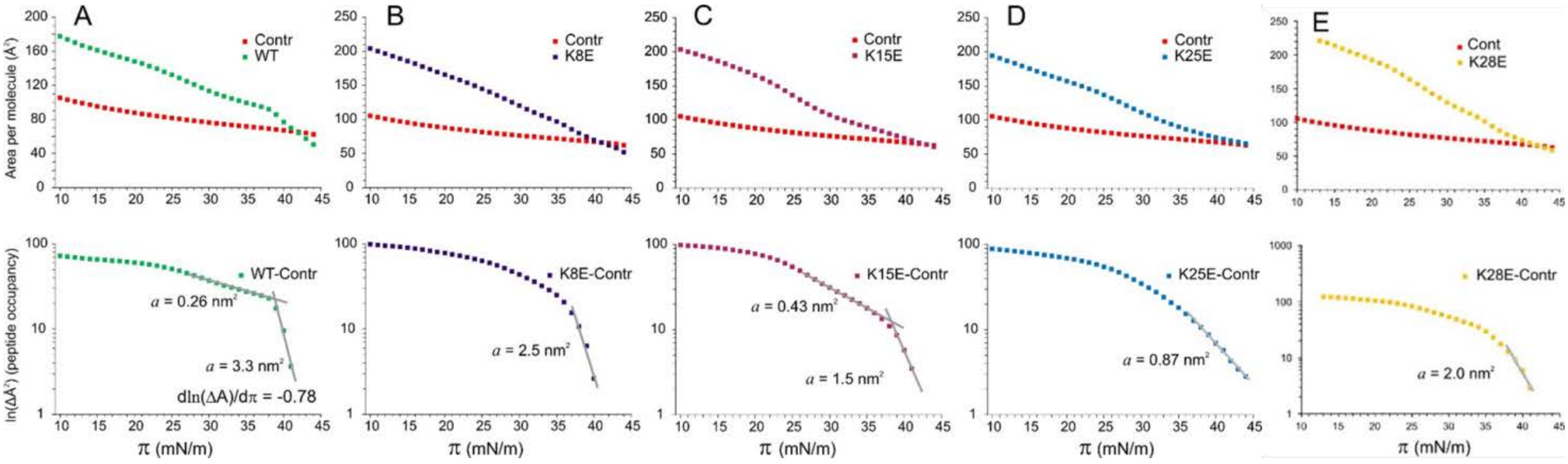

Figure S10. Plots of the area vs pressure (top panels) between the control and peptide curves for WT (A), normal activity variants K8E (B) and K28E (E), and the two least active variants K15E (C) and K25E (D). These plots illustrate partitioning of peptides into the monolayer in the expanded state (low pressures) and expulsion back to the subphase at higher pressures. The WT isotherm intersects with the control monolayer near the πB, while the least active variant isotherms approach the control near the πB but never intersect. Conversion to the logarithm of the area vs pressure (bottom panels) provides a clearer representation of the transitions during compression. If we assume that the change of the log-area with increasing pressure represents either the displacement of the peptide to a shallower state or complete expulsion of the peptide to the subphase, the slope of the film compaction can be used to calculate the peptide contribution to cross-sectional area prior to the transition. The active peptides (A, B and E) are displaced by lateral pressure from positions with effective molecular areas of 3.4 ± 0.1, 3.0 ± 0.2 and 2.3 ± 0.2 nm^2, whereas the transitions in inactive peptides (C and D) are shallower and show smaller molecular area changes.

The peptide intercalated into the film takes up substantial area and its presence is evident in expanded films. Compaction of the monolayer by the barrier and increase of lateral pressure leads to partial expulsion of the peptide back to the solution. To visualize the area occupied by the peptide we re-plotted the pressure-area curves in area-pressure coordinates and presented the area difference in log scale (Fig. S10). Assuming that the area change is proportional to the probability of a peptide inserting into lipid p_{lip} while p_{bulk} (concentration in the bulk) is constant, one can write

$$K_{eq} = \frac{p_{lip}}{p_{bulk}} = e^{-(\Delta G + \pi a)/kT} \quad , \quad \text{so that} \quad kT(\ln p_{lip} - \ln p_{bulk}) = -\Delta G - \pi a$$

Differentiating with respect to π we obtain,

$$-kTd(\ln p_{lip})/d\pi = a$$

where *a* is the area occupied by the peptide molecule in the plane of the lipid film.

The bottom row in Figure S10 is a plot of the log of the area difference vs pressure for the WT and four variants with a range of inhibitory properties. The obvious difference between WT, K8E, and K28E, and the two weakened activity peptides is the character of the intersection of the corresponding isotherms with the control. The slope of the logarithmic difference area plot near that intersection also reflects that difference. The flattening of the isotherms for active peptides occurring in the vicinity of the πB is the property that means high compressibility in that region.

For WT GsMTx4 (Fig. S10, bottom panel), one can see that there is minimal total area change at pressures below 20 mN/m. However, above 20 mN/m, the monolayer with the peptide starts compacting faster showing two compaction rates. A shallow-slope, or "*slow expulsion*" with an area change of 0.26 nm^2 is observed at pressures between 25-37 mN/m. At 37mN/m the WT-harboring monolayer undergoes a sharp transition reflecting a massive displacement/expulsion of the peptide. The slope corresponds to a particle with a cross-sectional area a = 3.4± 0.1 nm^2. The two variants with normal activity (K8E and K28E) also show relatively large changes in cross-sectional area. In contrast, no sharp transitions were observed in compromised K15E or K25E, but near the πB, particles were effectively displaced with the slopes corresponding to smaller characteristic areas between 2.8 ± 0.4 and 0.82 ± 0.9 nm^2, respectively. Figure S10 D shows that the K25E variant is apparently not completely expelled as its isotherm shallowly approaches the control curve but never crosses it.

Supporting Figure S10

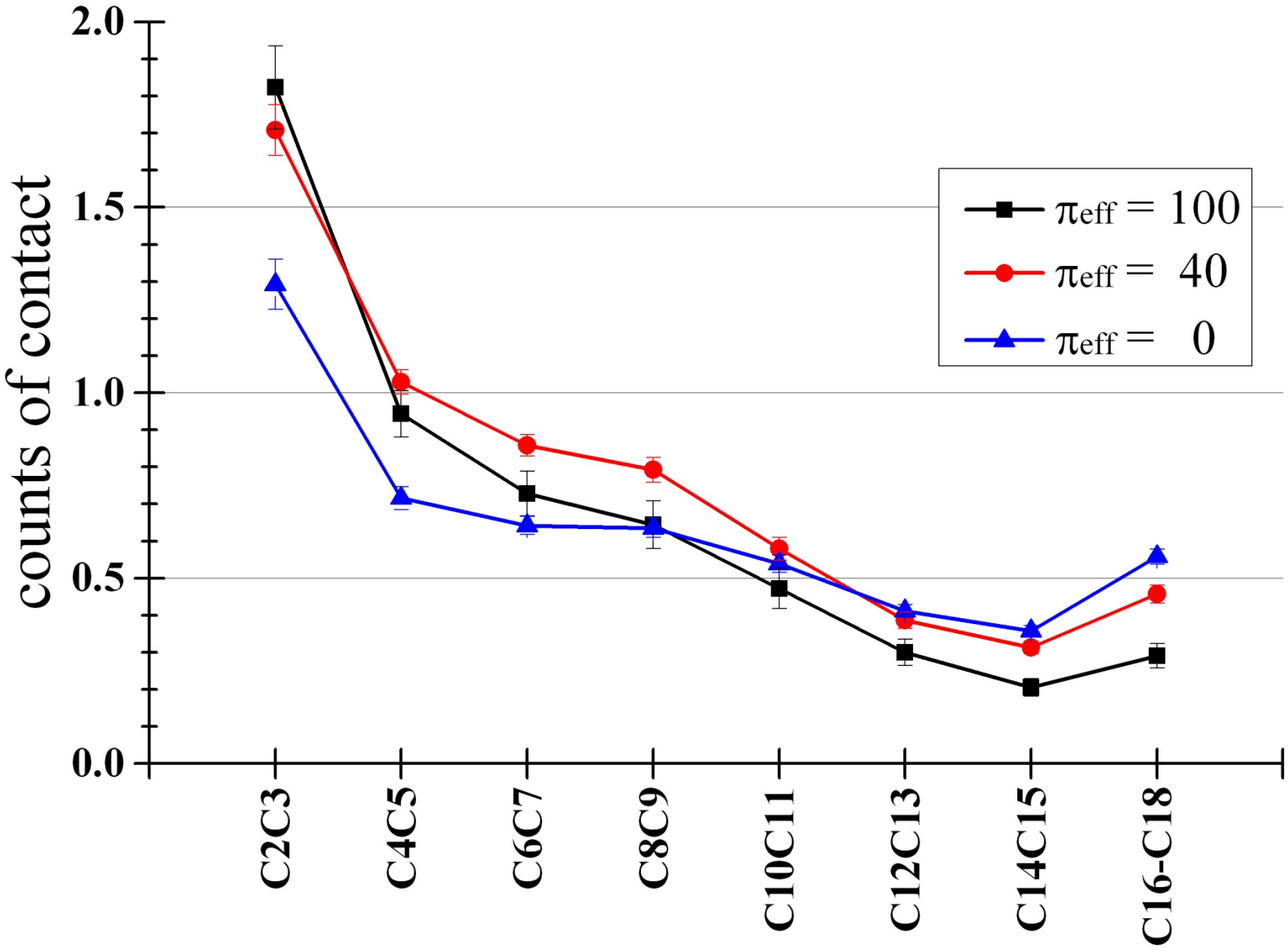

Figure S11. Simulation analysis of penetration depth of WT in the POPC monolayer based on the number of acyl chain (united) atoms in contact with WT. The y-axis shows the mean counts of the POPC acyl chain atoms (indicated in the x-axis) that were located within 3Å from any atoms of WT in the monolayer simulation data analyzed in Figure 7. Results for three distinct target membrane pressures (π_{eff}=0, 40 and 100) were shown. 'C2C3', for example, stands for the sum of the counts for C2 and C3. Error bars represent s.e. from the final 20ns of the trajectories.